



Improving weld penetration by two-TIG arc activated via mixing oxygen into shielding gas

Jia Zhang^{1,2} · Peize Shao^{1,2} · Xinxin Wang^{1,2} · Ding Fan^{3,4}

Received: 26 August 2022 / Accepted: 10 December 2022 / Published online: 22 December 2022
© The Author(s), under exclusive licence to Springer-Verlag London Ltd., part of Springer Nature 2022

Abstract

In order to improve welding efficiency of conventional TIG welding process, a new activating TIG (A-TIG) welding process, named activating arc two-TIG (AT-TIG) welding, was developed by using two-TIG arc activated via mixing minor oxygen into the shielding gas of the front welding torch. The effect of the oxygen flow rate, welding current carried by two tungsten electrodes, and welding speed on the weld formation were investigated for the bead-on-plate welding of SUS304 stainless steel. It was found that, compared to conventional TIG welding, this method can successfully obtain a markedly deepened weld penetration, even at a relatively higher welding speed. Mixing of O₂ into the argon shielding gas do not have a significant effect on the microstructure of the weld metal. The dramatically improved weld depth can be achieved at a lower oxygen flow rate and the corresponding impact toughness energy of the weld reaches as much as 92.3% of the workpiece. In addition, the modulation of the current proportions for each welding torch plays a prominent role in the weld formation, which was accounted by a numerical model that the current apportionment for each electrode results in the change of the arc plasma flow and thus the oxygen transfer process from the arc plasma to the weld pool. The predominant effect of the oxygen on the formation of the weld pool shape and the weld formation was demonstrated by a weld-bead-shift experiment. Therefore, the oxygen transfer process from the arc plasma to the weld pool and the mechanisms for enhancing the weld penetration in this welding process were clarified.

Keywords AT-TIG · Weld formation · Oxygen transfer · Mechanism

1 Introduction

Gas tungsten arc welding (GTAW), also known as tungsten inert gas (TIG) welding, is a versatile welding process and widely used in industry for its excellent weld formation, stable welding process, and high weld quality. However, its shallow penetration in single-pass welding causes relatively lower productivity compared to other arc welding processes

including submerged arc welding (SAW), gas metal arc welding (GMAW), and plasma arc welding (PAW). In addition, when the welding speed exceeds a critical value in high-speed GTAW, weld defects including undercut and humping are formed inevitably [1–3].

How to improve the GTAW efficiency has been a concern of the researchers for a long time and several technologies have been proposed, such as activating flux TIG (A-TIG) welding [4–7], ultrasonic-assisted TIG welding [8], high-frequency pulse TIG welding [9], and high-frequency magnetic controlled TIG welding [10]. Twin-arc TIG welding has been introduced by Japanese researchers firstly and applied in the construction of a large liquefied natural gas storage tank successfully [11]. A similar welding process was developed by Leng et al. [12] to use in high-speed welding; they indicated that this method can achieve steady welding process and sound weld under high welding speed. Pulse tandem TIG welding system was realized by Jiang et al. [13] for thin stainless steel plate, which can obtain good weld formation even if the welding speed is over 50 mm/s.

✉ Xinxin Wang
wang@cqut.edu.cn

¹ School of Materials Science and Engineering, Chongqing University of Technology, Chongqing 400054, China

² Chongqing Municipal Engineering Research Center of Higher Education Institutions for Special Welding Materials and Technology, Chongqing 400054, China

³ School of Materials Science and Engineering, Lanzhou University of Technology, Lanzhou 730050, China

⁴ State Key Laboratory of Advanced Processing and Recycling of Non-ferrous Metals, 730050 Lanzhou, China

Among them, A-TIG welding, characterized by low cost and remarkable deepened penetration, has been attracting worldwide attention since its advent [4–7, 14, 15]. Many investigations on the mechanism for enhanced weld depth in A-TIG welding have been reported, and it is to date generally accepted that the increased weld penetration for non-ferrous metals is induced mainly by arc constriction [16–19]; for steels, primarily by reversal of the Marangoni convection originating from the change in surface tension of the weld pool [20–24]. For the latter, both the experimental [25–27] and theoretical [7, 20, 24, 28, 29] investigations showed that the active elements, including O and S in the welding pool, reverse the Marangoni convection direction from an outward flow to an inward one. To date, the reversal of the internal flow behavior of the weld pool stemming from the activating element during welding and additive manufacturing (AM) was observed directly via in situ synchrotron X-ray transmitting technique by Aucott et al. [25], which demonstrated convincingly the predominant effect of the surfactant on the flow pattern within the molten pool. As a result, the heat from the arc is transported more to the weld center and bottom, and the penetration was increased dramatically. From this point of view, precise controlling of these minor elements in the weld pool in GTA welding process is critical for a satisfactory weld with deep penetration.

Inspired by the mechanisms of A-TIG welding, Fujii et al. [30] proposed advanced activating TIG (AA-TIG) welding; it was invented by using a double-shielding gas with the addition of some active gases into outer shielding gas, and a deep weld penetration was achieved. Fan et al. [31] developed arc-assisted activating TIG welding, in which the workpiece was pre-melted by assisting arc with lower current and gas mixture of argon and oxygen, so that the oxygen can be introduced to the weld pool in proceeding convectional TIG welding; as a result, the weld penetration was found

to increase markedly as well. This process was developed further to use in the welding of dissimilar steels [32].

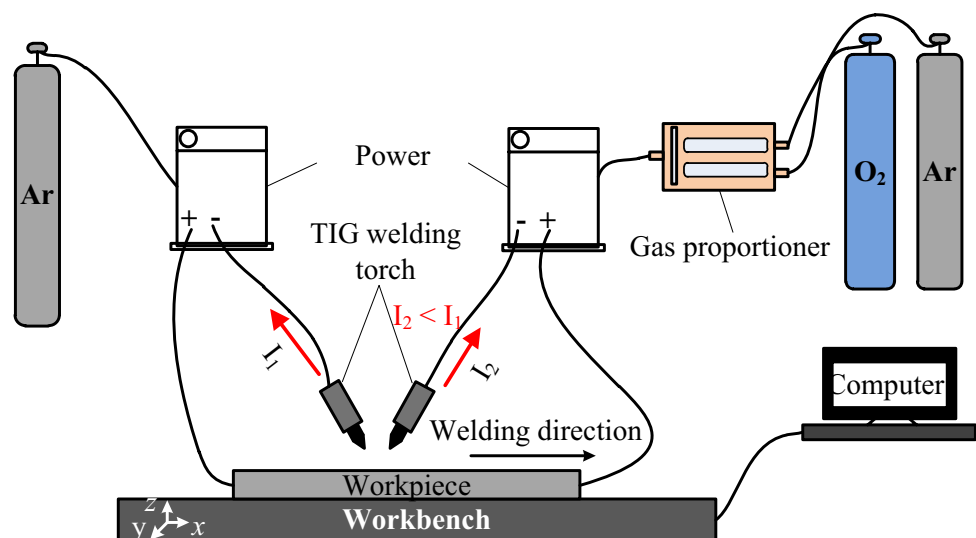
In this study, we advanced arc-assisted activating TIG welding and developed a new welding method named activating arc two-TIG welding (AT-TIG), in which two TIG welding torches were employed and oxygen was added to shielding gas of the front torch. Compared to the methods developed by Fan et al. [31, 32] and Fujii et al. [30], this process can be readily available and has a potential application in high-speed GTAW. In addition, the arc characteristics and thus the weld formation could be different from that in literature [33]. In the present paper, the effects of main process parameters, including oxygen flow rate, welding current for each electrode with equivalent total current, and welding speed, on the weld depth and width were investigated, and the weld microstructure and impact property are presented. Moreover, a computational fluid dynamics (CFD) model was used to elucidate the mass transfer of the oxygen in the two-TIG arc; meanwhile, a weld-bead-shift experiment was designed to account for the oxygen effect on the weld formation such that the oxygen transfer process from the arc plasma to the weld pool and the mechanisms for the increased weld penetration can be presented.

2 Methodology

2.1 AT-TIG welding process

The AT-TIG welding process is shown schematically in Fig. 1. Two TIG welding torches are used in tandem configuration and slanted to each other to form a certain angle in the plane perpendicular to the workpiece. Two independent welding power supplies are employed for each welding torch, and the welding current of the leading torch is less

Fig. 1 Schematic diagram of AT-TIG welding process



than that of the rear one. The shielding gas for the leading torch is mixed gas of argon and minor oxygen, while for the rear torch it is pure argon gas, such that the activating element oxygen is introduced to the two-TIG arc, and the arc plasma is “activated.” Then, the activating element oxygen can be transferred to the weld pool to increase the weld penetration. As the characteristic process parameters, tungsten electrode spacing (d) is defined as the horizontal distance between the tips of the two tungsten electrodes, while the arc length (L) is the vertical distance from the tip of the tungsten electrode to the workpiece, as shown in Fig. 1.

2.2 Experimental procedures

SUS304 stainless steel plate with dimension of 200 mm × 100 mm × 5 mm was selected as the workpiece for the bead-on-plate welding experiment. A direct current electrode negative (DCEN) polarity mode was selected for each of the welding torch; both of the torches were fixed in a workbench and the workpiece was moving at a set constant speed during welding. The cerium tungsten electrode with a diameter of 3.2 mm and a tip angle of 60° was used for each torch cooled by water. Basic welding process parameters are shown in Table 1, and the influence of the welding current, oxygen flow rate, and welding speed on the weld formation was examined. Prior to welding, the surface of the plate was ground using 80-grit flexible abrasive papers to remove the oxide layer and then cleaned by acetone.

After welding, all the weld beads were sectioned and the specimens for the weld shape observations were prepared and etched by aqua regia solution to reveal the bead shape and size as well as microstructure imaging. The cross-section, size, and microstructure of the weld beads were photographed and measured using an optical microscope. The mechanical properties of the weld were evaluated using a V-notch sharp impact test; the size of the impact test sample is 55 mm × 10 mm × 2.5 mm since the standard specimen cannot be extracted from the weld. Fracture surfaces of the destructed impact test specimens were observed by scanning electron microscope (SEM) to analyze the fracture behavior.

2.3 Computational fluid dynamics model

In the present research, the numerical model based on our prior research [33] was extended further to

three-dimensional (3D) case and employed to analyze the oxygen transfer in two-TIG arc. The primary points are briefly dictated herein. The approach for treating the binary composition diffusion in arc plasma for binary gas mixture was developed by Murphy [34] and was employed to treat diffusion of oxygen–argon mixture in the present model; the two tungsten electrodes were included in this model as well. As a simplified treatment, the workpiece and thus weld pool were not considered. Both the arc length and the tungsten electrode spacing were 3 mm, and the slanted angle for each electrodes is 30° to form a 60° angle between the two electrodes. Two cases, i.e., equal and unequal current for each electrode, were simulated for a same total current. The temperature distribution and oxygen mass fraction were exhibited for both cases, respectively; the latter was explained through the plasma flow properties. The thermophysical properties of the arc plasma in gas mixture of oxygen–argon for the model are both temperature and mass fraction dependent; they are referred in Refs. [35–37].

3 Results

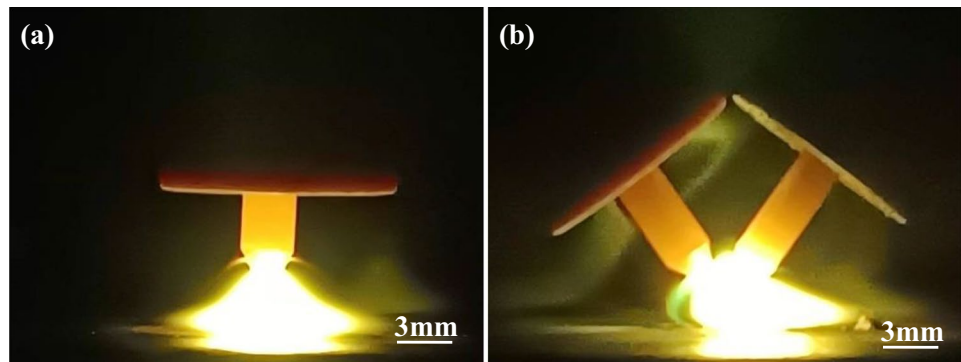
3.1 Arc shape

Figure 2 shows the arc shape in conventional TIG welding and AT-TIG welding under a welding current of 300 A. For the latter, the current for the left-side torch was 200 A, while that for the right-side torch was 100 A; the arc length was 3 mm and the Ar flow rate was 15 L/min. It can be seen in Fig. 2b that a well-coupled arc forms and its shape is no longer symmetric for AT-TIG arc, compared with the conventional TIG arc with a well-known bell shape in Fig. 2a; this appearance for AT-TIG arc is induced by the attraction of the Lorentz force of the two plasma jets as well as the stronger plasma jets from the tungsten electrode with higher current. Such stronger arc plasma flows along its electrode axis and toward the right side when it is hindered by the workpiece surface, so the whole arc extends apparently to the side of the tungsten electrode with the lower current. In fact, this flow property of the two-TIG arc has a crucial effect on the oxygen transfer in the arc plasma, which will be discussed in detail in Section 4.

Table 1 Basic welding process parameters

Welding current $I_1 + I_2$ (A)	Ar flow rate of the rear torch Q_1 (L/min)	Ar flow rate of the leading torch Q_2 (L/min)	O ₂ flow rate Q_3 (L/ min)	Welding speed V (mm/s)	Arc length L (mm)	Tungsten electrode spacing d (mm)
200 + 100	15	10	0.6	4	3	3

Fig. 2 Arc shape for **a** conventional TIG and **b** AT-TIG welding



3.2 Oxidation of tungsten electrodes

Oxygen mixed into the argon shielding gas makes the electrode tips oxidize inevitably. Oxidation of the electrode tip before and after welding with oxygen flow rate of 0.6 L/min is shown in Fig. 3; it is seen that the very tip of the electrode with shielding gas of argon and oxygen passing through becomes melted and blunt due to both the high temperature and oxidation, while that with argon gas keeps its initial shape well. The oxidation of the electrode tip will shorten the electrode application life and even affect the arc property and weld quality. Nevertheless, the melt size of electrode tip is less than 1 mm. From the results in the following section, it can be found that the weak oxidation of electrode tip plays a insignificant role in the weld formation and quality, although this change of the electrode tip may, to some extent, affect the arc plasma property.

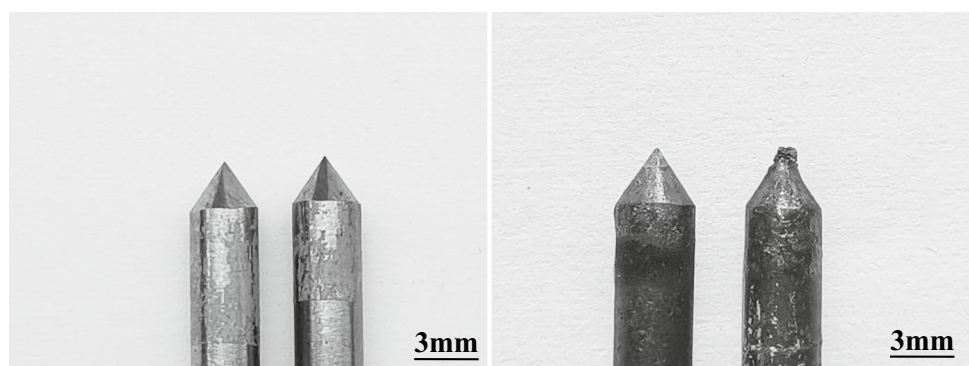
3.3 Weld formation

Comparison of the weld surface appearances and weld cross-sections under conditions listed in Table 1 for TIG welding, TIG welding with oxygen added into shielding gas, AT-TIG welding without oxygen, and AT-TIG welding with oxygen mixed are illustrated in Fig. 4, respectively.

As shown in Fig. 4a, the weld depth of conventional TIG welding is wide and shallow, and the weld surface is smooth and uniform. In contrast, the weld penetration for TIG welding with oxygen of 0.6 L/min is increased markedly, while the undercut occurs and the weld surface is oxidized severely, as seen in Fig. 4b. For AT-TIG welding without oxygen, the weld depth is shallower and weld width is narrower than those for TIG welding with pure argon, as presented in Fig. 4c. In AT-TIG arc welding, the weld penetration is the deepest with a full penetration, and the weld bead surface is smooth and uniform as well, as shown in Fig. 4d.

The weld depth and width are further plotted in Fig. 5. It can be seen that the weld depth and width of conventional TIG welding with pure argon denoted by “TIG” are about 3.0 and 14.4 mm, respectively; those of conventional TIG welding with oxygen mixed denoted by “TIG(O)” become 5.0 and 13.6 mm, respectively. For AT-TIG welding with pure argon denoted by “AT-TIG,” the width and depth are respectively 2.1 and 13.4 mm, whereas those for AT-TIG welding with oxygen mixed denoted by “AT-TIG(O),” the weld depth reaches 5.0 mm with a full penetration and the weld width reduces to 8.7 mm. As a whole, AT-TIG welding can achieve significant increased weld penetration and good weld surface appearance in analogous welding conditions.

Fig. 3 Oxidation of tungsten electrodes



(a) Before welding

(b) After welding

Fig. 4 Comparison of weld surface and cross-section formation for different cases under basic welding conditions

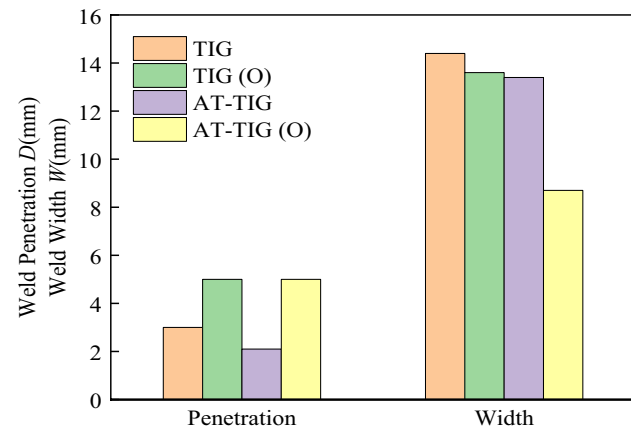
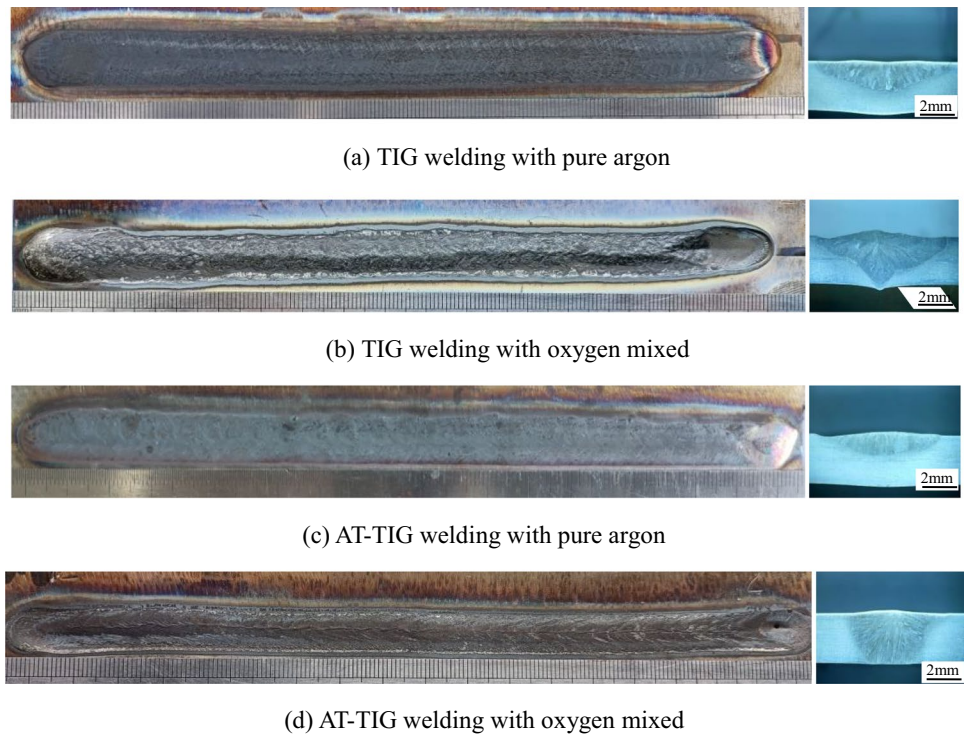


Fig. 5 Comparison of weld penetration and width for different cases under basic welding process conditions

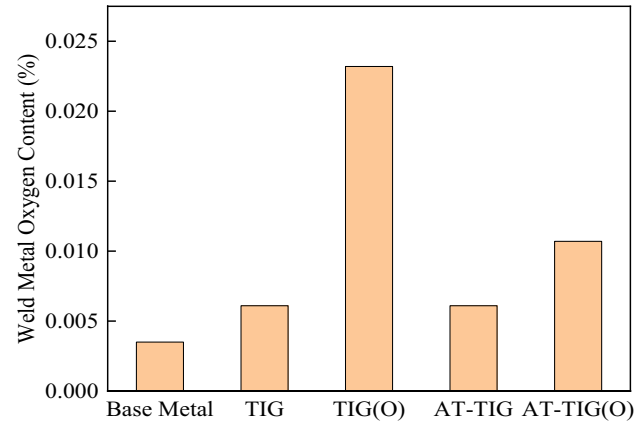


Fig. 6 Weld metal oxygen content for different cases under basic welding process conditions

The weld metal oxygen content for different cases corresponding to Fig. 4 is shown in Fig. 6. It can be seen that all the oxygen content of the samples for difference welding cases are greater than those of the base metal. The weld metal oxygen content of the conventional TIG welding with pure argon denoted by “TIG” is 0.0061%; that of the traditional TIG welding with oxygen denoted by “TIG(O)” reaches 0.0232%. For AT-TIG welding with pure argon denoted by “AT-TIG,” the weld metal oxygen content is 0.0068%, whereas for AT-TIG welding with

oxygen denoted by “AT-TIG(O),” the weld metal oxygen content is 0.0107%. Compared to conventional TIG welding with oxygen, the weld metal oxygen content of AT-TIG welding is at a relatively low level under the same welding conditions. It is obvious that the weld oxygen content of AT-TIG welding in much less than that of the TIG welding with the same amount of oxygen introduced into the shielding gas. The oxygen content in the weld of AT-TIG welding is close to that presented by Lu et al. [22] and keeps at a lower level.

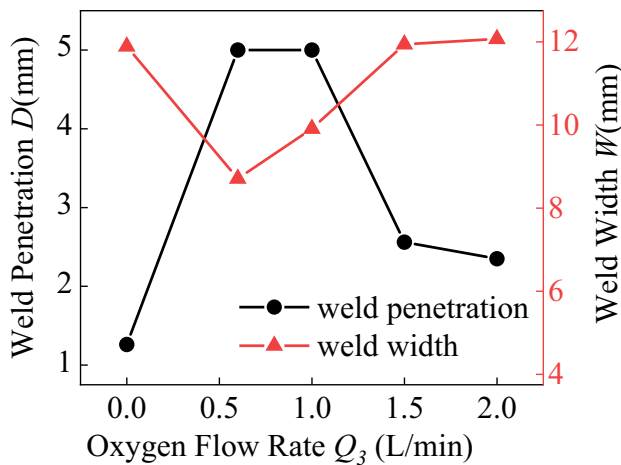


Fig. 7 Influence of the oxygen flow rate on the weld formation

3.4 Effect of the main process parameters on the weld formation

The effect of oxygen flow rate on the weld depth and width is shown in Fig. 7. The results show that with the increase in oxygen flow rate, weld penetration increases first and then decreases, while the weld width decreases first and increase subsequently. As the oxygen flow rate is 0.6 and 1.0 L/min, the weld depth is the deepest with a full penetration, while weld width is relatively narrow, only 8.7 and 9.9 mm, respectively. The paramount importance of the oxygen on the weld pool shape and size of steels has been investigated by many researchers from the aspect of both the theory and the experiment [20–22, 25–27, 38], respectively; it is now believed that the oxygen solution into the weld pool results in the change in temperature dependence of the surface tension of the weld pool from a negative value to a positive one, which generates inward Marangoni convection and thus increased weld penetration. This point will be discussed in detail in Section 4.2.

As the oxygen flow rate increases, the oxygen dissolved in the weld pool increases and the surface tension temperature $d\gamma/dT$ inverses [38], leading to a reversed Marangoni flow and inward heat convection; the more oxygen introduced into the weld pool, the stronger the inward heat convection and deeper weld depth becomes. At the oxygen flow rate of 0.6 and 1.0 L/min, the Marangoni flow is the most intensive and the weld penetration is the deepest. When the oxygen flow rate surpasses 1.0 L/min, there is an excess of the oxides over the weld pool surface, which means the surface tension of the molten metal becomes that of the oxides, and the influence of the oxygen on the weld pool surface tension diminishes and even vanishes, so the inward Marangoni convection of the weld pool weakens and weld depth decreases accordingly. Lu et al. [39] proposed a similar model to explain the oxide formation over the weld pool

and its hindering effect on the oxygen absorption by the weld pool.

The change in the weld width can also be explained by the melt flow within the weld pool; the stronger the inward Marangoni convection becomes, the more energy is transferred to the center of the weld pool, so less solid metal adjacent to the weld pool top area is melted, but more solid metal adjacent to the weld pool bottom is melted. As a result, the weld width becomes narrow and presents a minimum value under oxygen flow rate of 0.6 L/min. As a whole, the variation trend of the width with the increase of the oxygen flow rate is opposite to that of the change in weld penetration.

The effect of welding current on the weld depth and width is shown in Fig. 8. In this case, the total current is 300 A, and the current carried by each electrode varies. It can be seen that, with the increase in welding current of the rear torch (decrease in welding current of the leading torch), weld penetration increases first and then decreases, while weld width keeps increasing all throughout the range of the current.

According to the aforementioned analysis, it is believed that the weld penetration change here is induced by the oxygen concentration in the weld pool, which in this case results from the current change for the tungsten electrode. The influence of the electrode current on the oxygen transfer to the weld pool will be further discussed in Section 4.1. As for the increase in weld width, it is generated by the extension of the arc coverage over the weld pool when either of the electrode current increases.

The effect of welding speed on the weld depth and width is shown in Fig. 9. It can be seen that, with the increases of welding speed, both the welding penetration and width decrease, and weld surface formation keeps well. It is noticeable that when the welding speed is over 16 mm/s, the effect

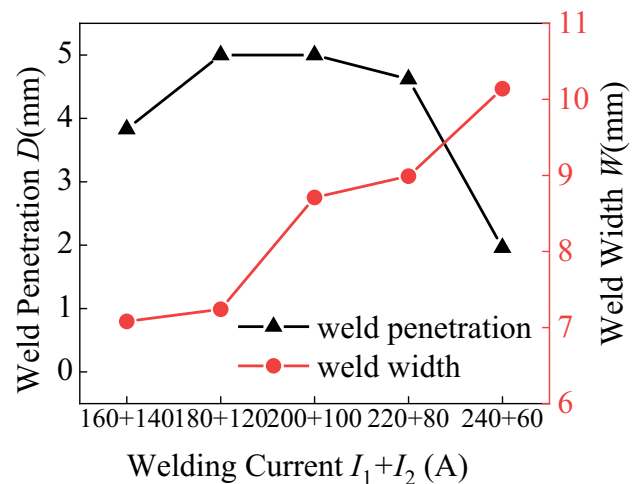


Fig. 8 Influence of the welding current on the weld formation

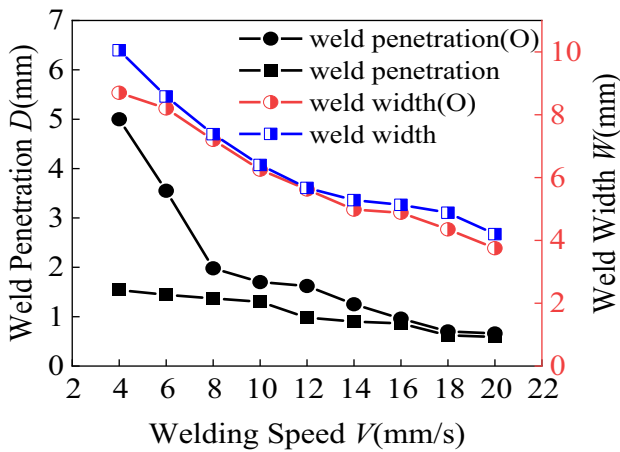


Fig. 9 Influence of the welding speed on the weld formation

of the active elements oxygen on increasing weld penetration is not obvious.

A high welding speed will reduce the weld pool volume; also, it shortens the liquid weld pool retaining time and decreases the oxygen dissolved into the liquid pool. Therefore, there is no adequate time for oxygen to exert its influence on the weld pool, and weld penetration and width do not significantly change when the welding speed is over a critical value.

3.5 Microstructure and mechanical property

The effects of oxygen on the microstructure of the weld metal were investigated by comparing the microstructure under oxygen flow rate of 0 and 0.6 L/min, respectively, as shown in Fig. 10. It is clear that weld microstructure consists of a large amount of austenite and a small amount of δ -ferrite; the latter presents both the vermicular and lathy types. Overall, the mixing of O_2 gas into the shielding gas has no significant effects on the microstructure of the weld metal.

The effect of the oxygen flow rate on the impact toughness is drawn in Fig. 11. As shown, as the oxygen flow rate in the shielding gas increases, the impact toughness of the weld

Fig. 10 Microstructure of weld metal for oxygen flow rate of **a** 0 L/min and **b** 0.6 L/min

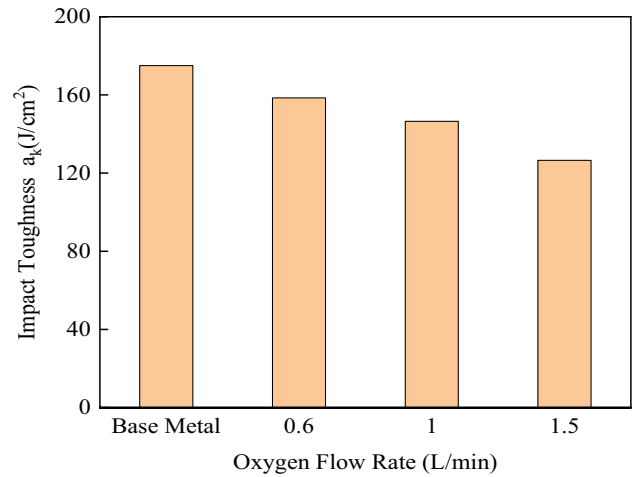
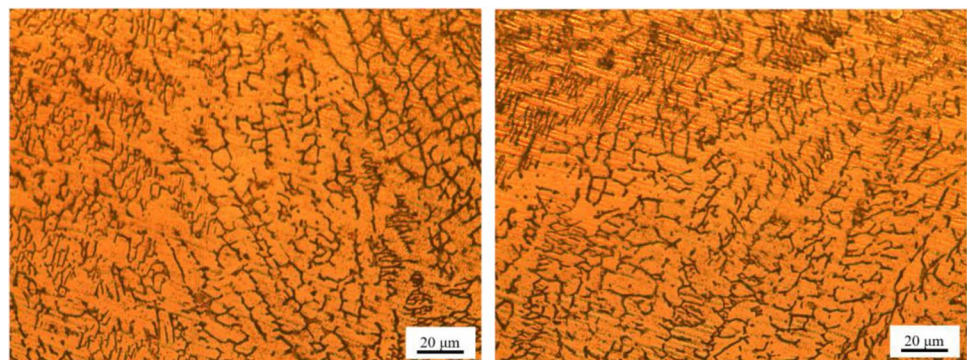
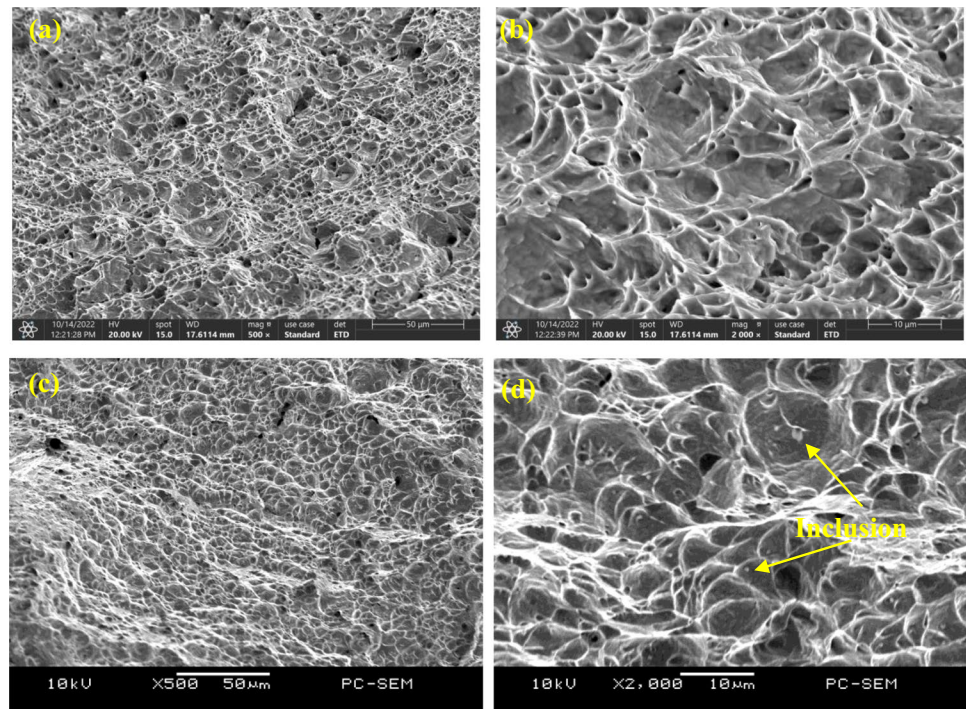


Fig. 11 Influence of the oxygen flow rate on the impact toughness of the weld

metal reduces. All the impact toughness of the samples for different oxygen flow rates are lower than those of the base material. The impact toughness of substrate is 175J/cm^2 ; when the oxygen flow rate is 0.6, 1.0, and 1.5 L/min, the impact toughness drops to 158.5J/cm^2 , 146.5J/cm^2 , and 126.5J/cm^2 , respectively. However, a full weld penetration can be obtained in the present case when the oxygen flow rate is 0.6 L/min, which is corresponding to the impact toughness of 158.5J/cm^2 , as much as 92.3% of the workpiece.

Furthermore, the impact fracture surface of the AT-TIG welding with pure argon and AT-TIG welding with oxygen was analyzed by SEM, and the fractography microstructure is shown in Fig. 12. It is seen that the impact fractured surface for the two cases present dimples which means a ductile fracture mode. For the AT-TIG welding with pure argon, it is shown in Fig. 12a and b that the fractured surface have the smaller dimples without significant oxide impurities or inclusions. As for the AT-TIG welding with oxygen mixed, as shown in Fig. 12c and d, there are inclusions with different sizes in dimples; since the oxygen is introduced and dissolved into the weld pool, a variety of oxides can be formed

Fig. 12 Impact fracture morphologies of impact samples: **a, b** AT-TIG welding with pure argon; **c, d** AT-TIG welding with oxygen (0.6 L/min)



and trapped in the weld during rapid solidification of the weld pool. This is responsible mainly for the impact toughness reduction of the weld metal, according to the research of Refs. [40–42].

4 Discussion

4.1 Mass transfer of oxygen in two-TIG arc

The main mechanism for enhancing the weld penetration in A-TIG welding is reversal of the Marangoni convection of the weld pool, and the surface-active elements, such as oxygen and sulfur, can significantly change the Marangoni convection direction [4, 6, 20, 25, 29]. Therefore, mass transfer of the oxygen from the arc plasma to the weld pool and its distribution over the weld pool surface is foremost to reveal its effect on the weld shape variation in AT-TIG welding. All factors that affect weld pool oxygen content can change temperature coefficient of the surface tension and thus the weld pool shape.

Based on our prior investigation [33], the oxygen transfer in AT-TIG arc plasma was presented by extending the 2D model to a 3D one. The argon flow rate is 15 L/min for each of the welding torches, and the oxygen flow rate is 1 L/min, which is corresponding to an oxygen volume fraction of 5.41% and a mass fraction of 6.67%, respectively. Two cases of the welding current, i.e., 120 A + 120 A and 160 A + 80 A, are considered to exhibit the effect of the current partition of the two electrodes on the oxygen transfer in the

arc plasma. Both the tungsten electrode spacing and the arc length are 3 mm; the diameter of the tungsten electrode is 3.2 mm with a conical tip angle of 60°.

Figure 13 draws the arc temperature distribution and the distribution of the oxygen mass fraction for the current of 160 A + 80 A. It can be seen in Fig. 13a that an asymmetric arc forms due to the unequal current carried by each electrode. The peak temperature of the arc plasma in Ar–5.4% O₂ gas mixture is over 15,000 K close to the tip of the tungsten electrode with higher current. As seen in Fig. 13b, the oxygen concentrates mainly around the electrode with lower current; more importantly, the oxygen mass fraction near the anode (weld pool) under this electrode reduces to a rather low level. Nevertheless, oxygen transported to the front part (right side) of the weld pool is more than that to the rear part (left side) of the weld pool in AT-TIG welding since the welding torch with lower current is in the front, as shown in Fig. 1.

Figure 14 illustrates the temperature and oxygen mass fraction distributions in the case of 120 A + 120 A. In contrast to that in the above case, the arc plasma is symmetric except that very near the electrode tips, where the temperature close to the electrode with oxygen mixed into the shielding gas is slightly higher, as shown in Fig. 14a. As can be seen in Fig. 14b, oxygen concentrates more significantly to the side from which the oxygen was introduced into the shielding gas, and its mass fraction close to the electrode of this side is higher than that in input shielding gas because of the stronger diffusion induced by the temperature gradient and weaker convective mass transfer,

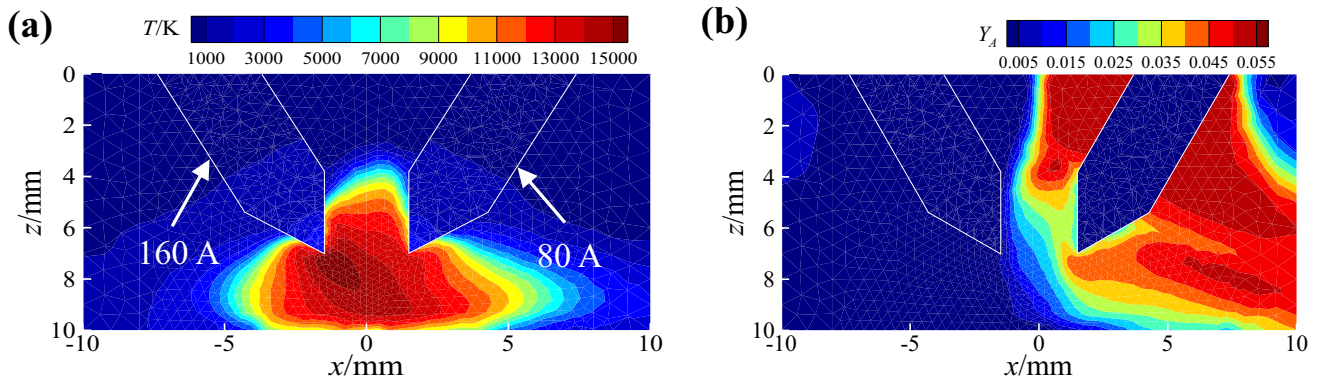


Fig. 13 Distributions of **a** temperature and **b** oxygen mass fraction of AT-TIG arc in Ar-5.41% O₂ gas mixture for welding current of 160 A + 80 A

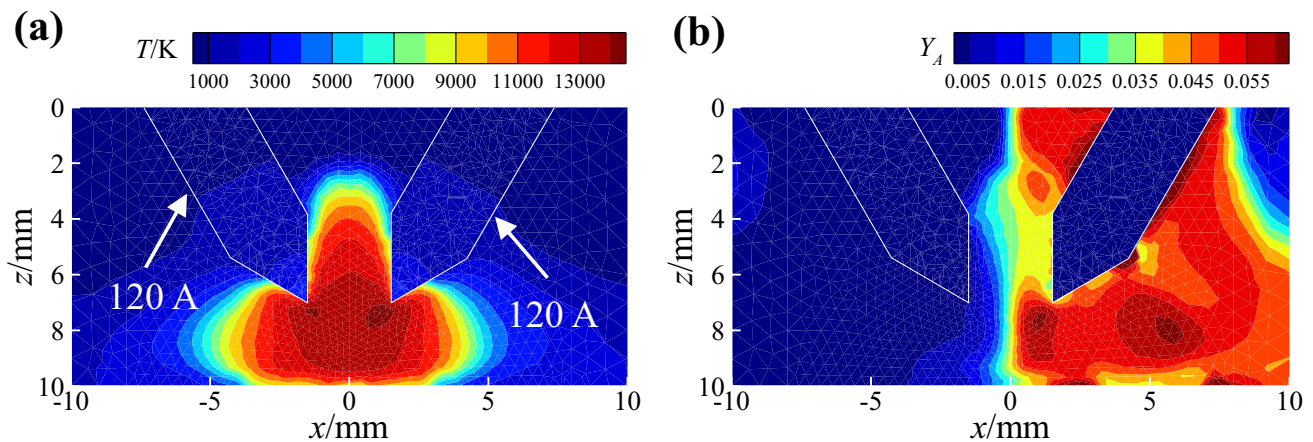


Fig. 14 Distributions of **a** temperature and **b** oxygen mass fraction of AT-TIG arc in Ar-5.41% O₂ gas mixture for welding current of 120 A + 120 A

as suggested in [33] and discussed following. It is more noticeable that the oxygen concentration near the anode (weld pool) is much higher than that in the case of 160 A + 80 A current.

The difference between the above oxygen distributions is caused by the plasma flow in different cases of current partition for each electrode. As drawn in Fig. 15a, the plasma flow from the electrode with higher current is much stronger than that from the other electrode for the case of 160 A + 80 A current, so more oxygen is transported by such plasma flow along its moving direction and, as a result, blown to the periphery region of the arc column. In comparison, for the equal electrode current, the velocity magnitude of the plasma flow from each electrode is almost the same, seen in Fig. 15b, so the oxygen mass transfer by convection reduces greatly and its diffusion toward the arc center region becomes more pronounced.

Furthermore, we can give a detailed explanation for the effect of the electrode current partition on the weld width and penetration, as shown in Fig. 7. The closer the current level for each electrode, the more oxygen is transferred to the weld pool. Therefore, as the current of the front torch increases and that of the rear torch reduces, the oxygen transported by the plasma flow to the weld pool decreases progressively. Since there is an optimum value of the oxygen concentration in the weld pool for improving the weld penetration most profoundly, as shown by the effect of the oxygen flow rate on the weld formation in Fig. 6 and other relevant research in [43, 44], the weld depth is able to reach a maximum at a certain current partition of each electrode in AT-TIG welding. Therefore, the minor oxygen introduced into the weld pool can be modulated and controlled in virtue of varying the current for each electrode to obtain a desired weld penetration and property, while keeping equivalent total current and thus almost unchanged heat input.

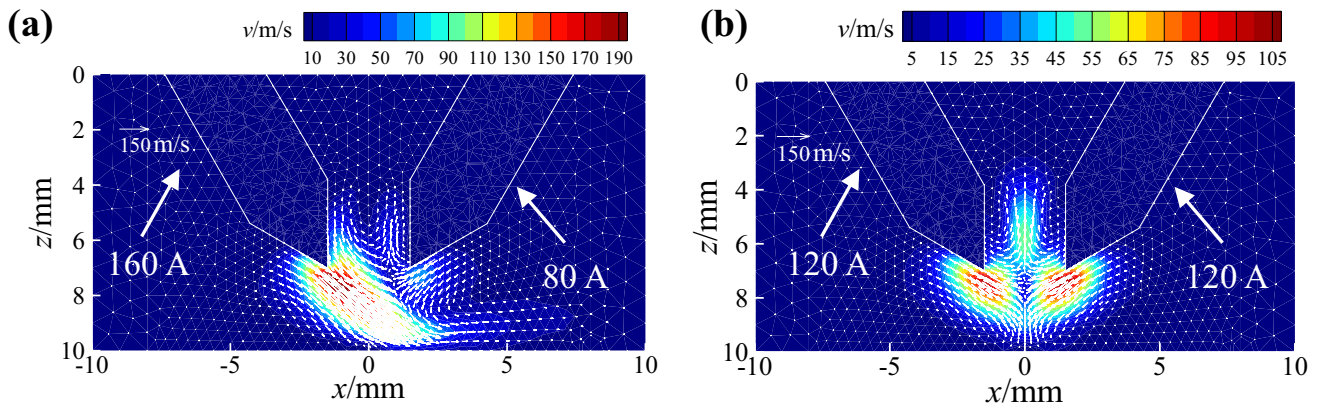


Fig. 15 Flow velocity of arc plasma in Ar–5.41% O₂ gas mixture for welding current of a 160 A + 80 A and b 120 A + 120 A

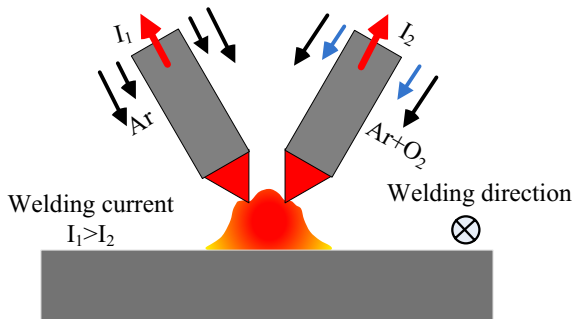


Fig. 16 Schematic diagram of weld bead center line shift experiment

4.2 Molten metal flow within the weld pool

In order to validate the effect of oxygen on the flow pattern in the weld pool and weld variation, a weld-shift experiment was designed and carried out; the schematic diagram is shown in Fig. 16, and the details of the welding process parameters are listed in Table 2. Welding direction is vertical to the line through the electrodes' tips, i.e., the two torches are moving in parallel arrangement, and the surface and cross-section of the weld without and with oxygen are presented in Figs. 17 and 18, respectively. The results show that the weld formation is not symmetrical and is shifted to the side with lower electrode current if oxygen is not

Table 2 Welding process parameters

Welding current $I_1 + I_2$ (A)	Ar flow rate of the rear torch Q_1 (L/min)	Ar flow rate of the leading torch Q_2 (L/min)	O ₂ flow rate Q_3 (L/min)	Welding speed V (mm/s)	Arc length L (mm)	Tungsten electrode spacing d (mm)
200 + 100	15	10	0.6	6	3	3

Fig. 17 Macrograph of weld center line shift for a pure argon shielding and b oxygen mixed

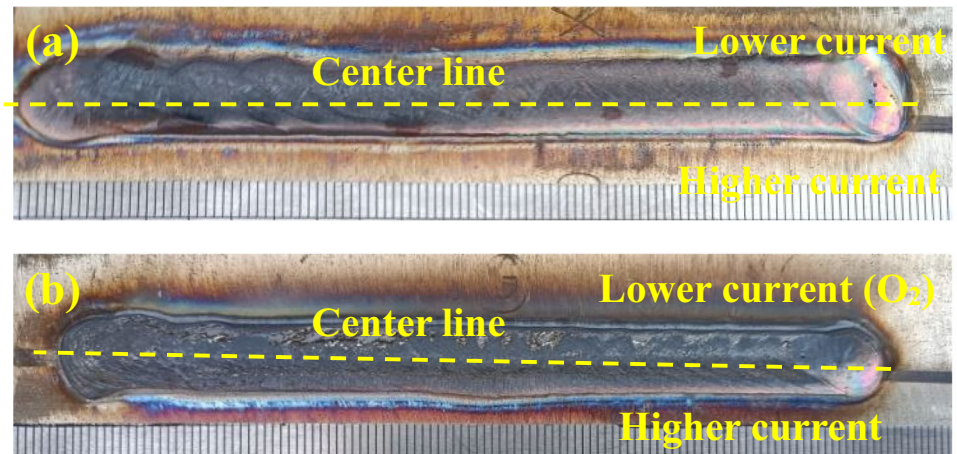
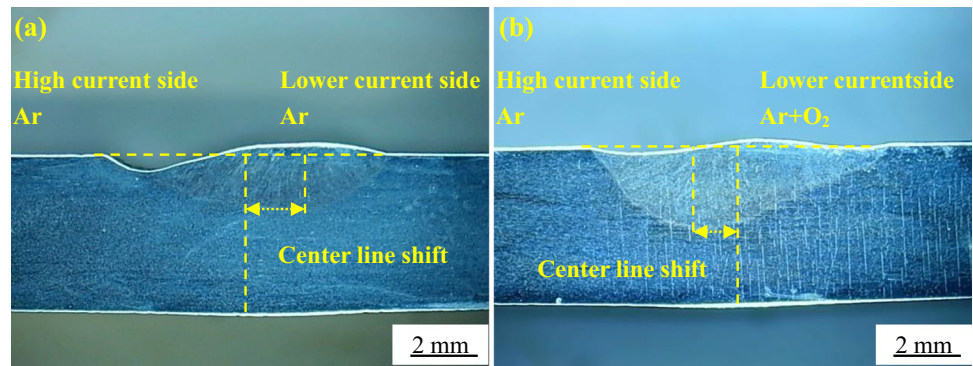


Fig. 18 Cross-section of weld profile for **a** pure argon shielding and **b** oxygen mixed



mixed, as shown by the weld appearance and cross-section in both Figs. 17a and 18a, respectively, while the weld bead is shifted to the side with higher electrode current when oxygen is mixed, as shown in Figs. 17b and 18b. It is noted that the position of the maximum weld penetration for the weld without oxygen is not centered on the weld seam and shifts to the side of lower electrode current about 1.91 mm, whereas that for the weld with oxygen shifts to the other side, i.e., the side with higher current, about 1.44 mm.

The weld shift can be accounted schematically via Fig. 19. When the oxygen is not introduced, the surface tension of the weld pool γ drops as the temperature increases, i.e., surface tension temperature coefficient $\partial\gamma/\partial T$ is negative, so the Marangoni shear force over the weld pool surface is directed from the center of the weld pool to the edge of that, and thus the molten metal flow in the weld pool is outward with the combination of the Marangoni shear force and the plasma shear force, as shown in Fig. 19a. Comparatively, as the oxygen is added and its content at the weld pool surface exceeds some threshold, surface tension temperature coefficient of the weld pool on the lower electrode current side becomes positive and the direction of the Marangoni

force becomes opposite, resulting in the reversed flow pattern, or Marangoni convection, within the weld pool; while on the side of higher current, the fluid flow at the weld pool surface is still outward. As a whole, both the molten metal and heat at the weld pool surface are transported more from the side under electrode with lower current to that with higher current, then downward to the weld pool bottom and giving rise to a weld shift to the side with higher current, as shown in Fig. 19b. Although the plasma shear force still exists, Marangoni shear force is the predominant factor since its effect is larger than the former, as suggested in Refs. [20, 24], and [44]. Noted that the weld penetration in this experiment is less than that in AT-TIG welding, we believe such difference is caused by the welding direction in the experiments. In the validation experiment, the welding direction is designed to be vertical to the line through the electrodes' tips, i.e., the two torches are moving in a parallel arrangement, while in AT-TIG welding, the torches are arranged in tandem type. For the former, the oxygen is introduced from the side in the welding direction, so the oxygen element dissolved into the weld pool is less than that in the latter case, where the oxygen is mixed ahead of the weld pool; on the

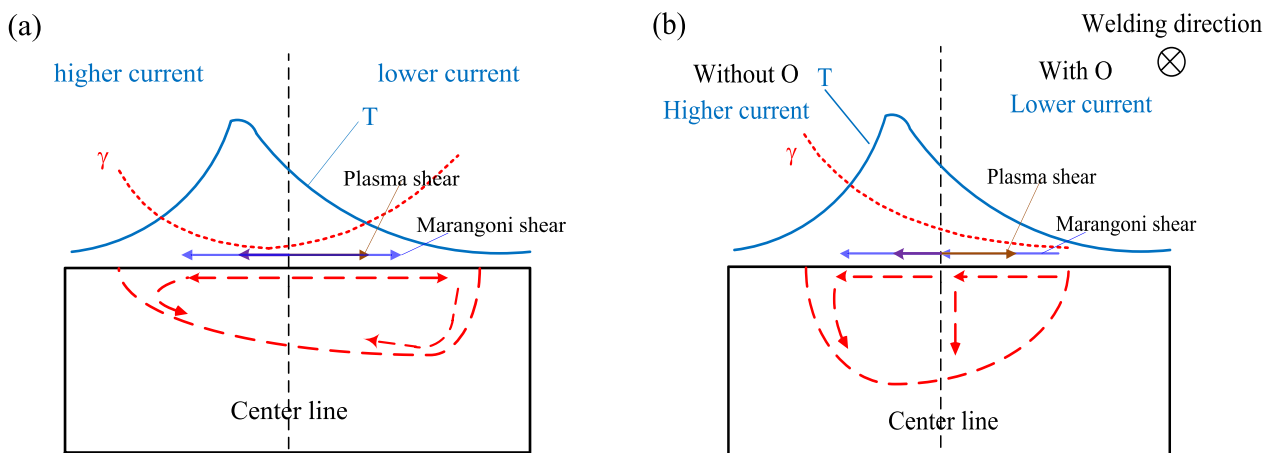


Fig. 19 Schematic diagram of metal flow within the weld pool for **a** Ar and **b** Ar-O₂

other hand, the flow of the weld pool in the former case is not inward completely, as shown in Fig. 19b, and the heat transferred to the weld pool center is less than that in the AT-TIG welding. For the two reasons, the penetration shown in Fig. 18b is less than that in Fig. 8.

Regarding the weld shift to the side of lower current without oxygen added, we believe that this phenomenon is induced by the asymmetrical distributions of the Marangoni force and plasma shear force at the weld pool surface. Especially the latter, arising from the high-velocity plasma flowing over a relatively quite low motion velocity of the weld pool surface, makes a great difference on the weld pool formation when the current changes. As seen in Fig. 15b, the plasma flow adjacent to the anode in this case has a significant tendency to push the molten metal of the weld pool from high current side to the lower current side. As a result, both the melt and the heat were transported more to the lower current side, leading to a weld shift to this side and an undercut at higher current side.

5 Conclusion

A high-efficiency welding process named AT-TIG welding is developed and the effects of the main process parameters on the weld formation are investigated, and the mechanical property and microstructure of the weld are presented; furthermore, the oxygen transfer process in the arc plasma is modeled and finally the weld pool formation mechanisms are revealed, and the conclusions can be drawn as follows:

1. Compared to conventional TIG welding, weld penetration can be enhanced significantly in AT-TIG welding, even at a relatively higher welding speed.
2. Optimum oxygen can be controlled by the oxygen flow rate as well as the current carried by each electrode, to achieve a desired weld formation while ensuring the weld mechanical property at low oxygen flow rate.
3. Electrode current partition for the same total current plays a critical role in the arc plasma flow and thus the oxygen mass transfer from the arc plasma to the weld pool.
4. Reversal of the Marangoni convection caused by the oxygen and induced convective heat transfer within the weld pool are the dominant factors in determining the weld formation in AT-TIG welding.

Author contribution JZ: investigation, methodology, writing—original draft. PS: investigation, methodology. XW: methodology, funding acquisition, writing and revising, data curation. DF: methodology, supervision.

Funding The National Natural Science Foundation of China (No. 51705054) and The Scientific and Technological Research Program of Chongqing Municipal Education Commission (No. KJQN202101135).

Data availability All data generated or analyzed during this study are included in this published article. The experimental data in this article can be used for scientific research, teaching, etc.

Declarations

Ethics approval The authors state that the present work is in compliance with the ethical standards.

Consent to participate and for publication All the authors listed have approved the manuscript, consented to participate, and consented for publication.

Conflict of interest The authors declare no competing interests.

References

1. Mendez PF, Eagar TW (2003) Penetration and defect formation in high-current arc welding. *Weld J* 82:296–306. <https://doi.org/10.1007/s00421-008-0955-8>
2. Soderstrom E, Mendez P (2006) Humping mechanisms present in high speed welding. *Sci Tech Weld Join* 11:572–579. <https://doi.org/10.1179/174329306X120787>
3. Meng XM, Qin GL, Zou Z (2016) Investigation of humping defect in high speed gas tungsten arc welding by numerical modeling. *Mater Design* 94:69–78. <https://doi.org/10.1016/j.matdes.2016.01.019>
4. Dhandha KH, Badheka VJ (2015) Effect of activating fluxes on weld bead morphology of P91 steel bead-on-plate welds by flux assisted tungsten inert gas welding process. *J Manuf Process* 17:48–57. <https://doi.org/10.1016/j.jmapro.2014.10.004>
5. Cai YC, Luo Z, Huang ZY, Zeng YD (2016) Effect of cerium oxide flux on active flux TIG welding of 800 MPa super steel. *J Mater Process Tech* 230:80–87. <https://doi.org/10.1016/j.jmatp.rotec.2015.11.008>
6. Kulkarni A, Dwivedi DK, Vasudevan M (2018) Study of mechanism, microstructure and mechanical properties of activated flux TIG welded P91 Steel-P22 steel dissimilar metal joint. *Mat Sci Eng A-Struct* 731:309–323. <https://doi.org/10.1016/j.msea.2018.06.054>
7. Unni AK, Muthukumar V (2021) Numerical simulation of the influence of oxygen content on the weld pool depth during activated TIG welding. *Int J Adv Manuf Tech* 112:467–489. <https://doi.org/10.1007/s00170-020-06343-1>
8. Sun QJ, Lin SB, Yang CL, Zhang GJ (2009) Penetration increase of AISI 304 using ultrasonic assisted tungsten inert gas welding. *Sci Tech Weld Join* 14:765–767. <https://doi.org/10.1179/136217109X12505932584772>
9. Cook GE, Eassa EH (1985) The effect of high-frequency pulsing of a welding arc. *IEEE T Ind Appl* 5:1294–1299. <https://doi.org/10.1109/TIA.1985.349557>
10. Nomura K, Ogino Y, Haga T, Hirata Y (2010) Influence of magnet configurations on magnetic controlled TIG arc welding. *Trans JWRI* 39:209–210
11. Kobayashi K, Nishimura Y, Iijima T, Ushio M, Tanaka M, Shimamura J, Ueno Y, Yamashita M (2004) Practical application of high efficiency twin-arc TIG welding method (SEDAR-TIG) for PCLNG storage tank. *Weld World* 48:35–39. <https://doi.org/10.1007/BF03266441>

